Astron. Astrophys. 75, 326–339 (1979)

ASTRONOMY AND ASTROPHYSICS

# Infrared Emission of Dusty H II Regions

A. G. G. M. Tielens[1] and T. de Jong[2]

[1] Sterrewacht, Huygens Laboratorium, Wassenaarseweg 78, 2300 RA Leiden, The Netherlands
[2] Astronomical Institute, Roeterstraat 15, 1018 WB, Amsterdam, The Netherlands

Received April 10, 1978

**Summary.** We have developed a numerical program to calculate the infrared emission from dust in compact H II regions. We assume that the dust consists of spherical monosize graphite, silicate and dirty ice particles. The relative amounts and the sizes of the dust particles are found by roughly fitting the observed wavelength dependence of the interstellar extinction curve and the albedo curve. We consider a spherical H II region ionized by a central star and surrounded by a dense neutral shell. We solve the combined ionization equilibrium of Hydrogen and Helium inside the H II region taking into account the absorption of ionizing (stellar and diffuse) photons by dust particles. We calculate the temperatures of individual dust particles by solving the heat balance, treating separately the ionizing stellar photons, the non-ionizing stellar photons and the recombination and cooling photons emitted by the ionized gas. The infrared spectrum is calculated by integrating the dust emission over the H II region and the dense neutral shell. A model for W3A/IRS1, one of the best studied compact H II regions, is constructed. This model has a central cavity, which is devoid of gas and dust, with a radius of about 2/3 the radius of the H II region. From a comparison of theoretical spectra with the observed near-infrared spectrum of W3A/IRS1 we find that the dust inside the H II region must be strongly depleted ($\delta \lesssim 0.1$). The spectrum is much broader than a black body spectrum because of the coexistence of particles of different dust materials and because of gradients in the dust temperature distributions. Finally, we find that the central exciting star of W3A/IRS1 is a hot O star with $T_{\rm eff} \simeq 50{,}000$ K and $L_* \simeq 4.5\ 10^5\ L_\odot$. This star contributes only about 30% of the total infrared luminosity of W3 (main component). We suggest that the remaining 70% is emitted by the nearby infrared source W3/IRS5 which probably contains a strongly obscured bright O star.

**Key words:** compact H II regions – infrared radiation – interstellar dust properties

## 1. Introduction

Most compact H II regions show emission at infrared wavelengths ($5\ \mu < \lambda < 1$ mm) in excess of the expected emission from free-free transitions in the ionized gas. This is generally attributed to emission from dust particles heated by stellar and nebular photons. The observations show that most H II regions have similar sizes at near-infrared and radio wavelengths. The near-infrared and radio surface brightness distributions of some H II regions that have been mapped in detail, are almost identical. This suggests a very close correlation between dust and gas emission.

The distribution and the amount of emitting dust is still a controversial issue. There exists a general correlation between the integrated radio and far-infrared flux densities (Harper and Low, 1971; Jennings, 1975). On the basis of this correlation the optical depth of the dust for ionizing photons has been estimated. The results suggest that in a large number of H II regions the dust-gas ratio inside the ionized region is comparable to the value in the general interstellar medium (Pottasch, 1974; Panagia, 1974). On the other hand the close correlation of the near-infrared and radio surface brightness distributions suggests that the resonantly scattered Lyman alpha photons dominate the heating of the dust inside the ionized region. This implies that the dust-gas ratio is much lower than in the general interstellar medium (Wright, 1973; de Jong, 1976). The apparent contradiction between these results can be reconciled by realizing that luminous protostars or young stars which do not contribute to the radio emission, because their H II regions are still optically thick, may contribute appreciably to the observed far-infrared luminosity. Thus the ultraviolet optical depths derived by comparing radio and infrared fluxes may be severely overestimated. As we shall argue in this paper a more detailed model of one of the best studied compact H II regions supports the earlier conclusion that the dust is strongly depleted inside the H II region.

In an earlier study we attempted to theoretically fit group properties derived from near-infrared and radio observations of resolved compact H II regions (de Jong et al., 1975). However, the large number of free parameters involved makes it difficult to draw firm conclusions. Therefore, we decided to fit the infrared spectrum and the surface brightness distribution of one particular H II region, using the radio observations as additional constraints. We chose W3A/IRS1 because it is one of the best-studied compact H II regions, in the radio as well as in the near-infrared (Wynn-Williams, 1971; Wynn-Williams et al., 1972; Harris and Wynn-Williams, 1976). In our earlier study we used a highly idealized dust model consisting of a solid with one infrared resonance at 10 μ or 50 μ. Since the shape of the spectrum turns out to depend strongly on the wavelength dependence of the absorption efficiencies of the emitting dust-particles, we decided to use a more realistic dust model. We assumed that the dust consists of a mixture of graphite, silicate, and ice particles. In order to limit the number of free parameters in the calculation, we first fixed the sizes and the relative abundances of these dust particles by fitting the observed interstellar extinction and albedo curves.

*Send offprint requests to:* A. G. G. M. Tielens

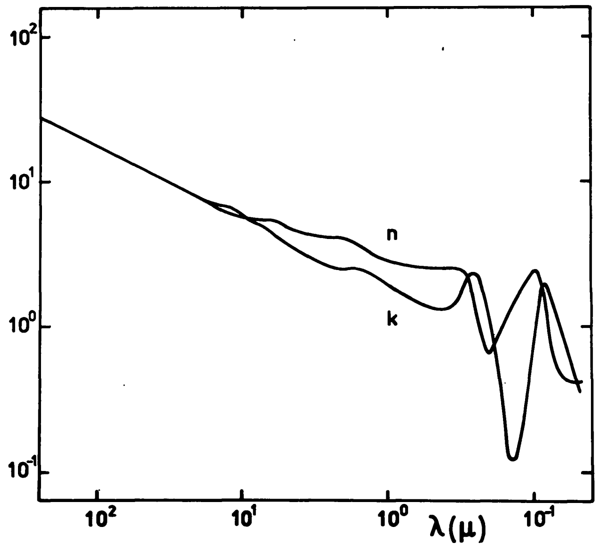


**Fig. 1.** The adopted optical constants of graphite

The paper is organized as follows. In Sect. 2 we specify the adopted optical properties of graphite, silicate, and ice. In addition we describe how we determine the sizes and the relative abundances of these particles. In Sect. 3 we describe how we calculate the ionization structure of an H II region containing Hydrogen, Helium, and dust. In Sect. 4 we discuss the different contributions to the heating of the dust particles and we describe how the infrared emission of an H II region is calculated. Our model for W3A/IRS1 is presented and discussed in Sect. 5. Finally, in Sect. 6 we summarize our main conclusions.

## 2. Adopted Dust Parameters

We have limited the chosen dust materials to graphite, silicate, and ice because there is some observational evidence that these materials are present in interstellar dust. By far the most outspoken feature of the interstellar extinction curve is the broad peak centered at 4.6 $\mu^{-1}$. This peak is usually attributed to plasma oscillations in uncoated spherical graphite particles with radii of about 200 Å (Gilra, 1972; Nandy et al., 1975). Two discrete absorption features at 9.7 μ and 3.1 μ have also been attributed to the interstellar dust. The 9.7 μ feature, seen in emission in the spectra of oxygen rich M giants (e.g. Woolf, 1975) and in absorption in protostellar objects like the BN object in Orion (Gillett and Forrest, 1973) has been ascribed to the SiO stretching mode in silicates. The rather sharp absorption feature at 3.1 μ observed in the spectra of heavily reddened protostellar objects is probably due to the OH stretching mode in ice (Gillett and Forrest, 1973).

In Fig. 1 we show the real and the imaginary parts of the complex refractive index, $m=n+ik$, of graphite. These data are derived from measurements by Taft and Phillipp (1965) of the dielectric constant $\varepsilon=\varepsilon_1+i\varepsilon_2$ of graphite, with the use of the relations $\varepsilon_1=n^2-k^2$ and $\varepsilon_2=2nk$ (e.g. Garbuny, 1965). The data of Taft and Phillip cover a range of photon energies from about 1 eV to 25 eV ($1\ \mu^{-1}\lesssim\lambda^{-1}\lesssim 20\ \mu^{-1}$). For energies between 0.1 and 1 eV they also present measurements of the conductivity $\sigma$ of graphite from which values of $\varepsilon_2$ can be obtained with the use of the relation $\varepsilon_2=2\sigma\lambda/c$ (e.g. Garbuny, 1965). For energies below 0.1 eV ($\lambda^{-1}\lesssim 0.1\ \mu^{-1}$) we have assumed that graphite behaves as a perfect conductor with a constant conductivity $\sigma=10^{15}\ \mathrm{s}^{-1}$ and optical constants $n=k=(\sigma\lambda/c)^{1/2}=1.8\,\lambda^{1/2}\,(\mu)\,(\mu)$. Whenever $n<k$ ($\varepsilon_1<0$) socalled "plasma oscillations" occur which result in strong peaks in $Q_{\mathrm{abs}}$, the absorption efficiency of small graphite particles (Gilra, 1972). One such peak is usually associated with the observed extinction maximum at $\lambda^{-1}=4.6\ \mu^{-1}$.

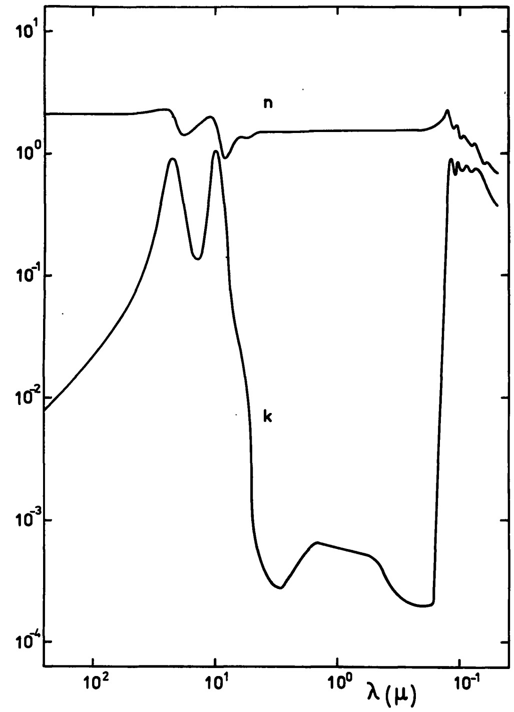


**Fig. 2.** The adopted optical constants of silicate

In Fig. 2 we have plotted the real and imaginary parts of the complex refractive index of a material that we shall call "silicate". These data are put together from two sources. For wavelengths longward of about 4000 Å we used the optical constants of basaltic glass, one of the terrestrial glasses studied by Pollack et al. (1973). The optical properties of the other rock samples analysed by Pollack et al. are very similar to basaltic glass. To our knowledge no optical constants of silicate type materials shortward of about 1000 Å are available in the literature. To complement the optical properties of our "silicate" down to about 500 Å we have used the data of amorphous quartz ($SiO_2$) obtained by Phillipp (1971) and connected these smoothly to the data of basaltic glass. This procedure does not violate the Kramers-Kronig relations because the connection occurs in a region of very low $k$. Moreover, the ultraviolet properties of oxydes are dominated by the behaviour of electrons which are strongly bound to the individual molecules in the solid, and $SiO_2$ is the most abundant molecule in basaltic glass. At wavelengths longward of 50 μ, where no measurements were available we have extrapolated the data applying elementary dispersion relations to the oscillator at 22 μ in basaltic glass, the strength and the width of which are given by Pollack et al. The optical properties of silicate are typical for a dielectric material, since always $k<n$.

In Fig. 3 we show the adopted optical constants of ice taken from a tabulation by Greenberg (1968). The long wavelength data have been extrapolated beyond 100 μ by fitting dispersion relations for Lorentz type oscillators at 46.5 and 62 μ to the data shortward of 100 μ. The real part of the refractive index asymptomatically

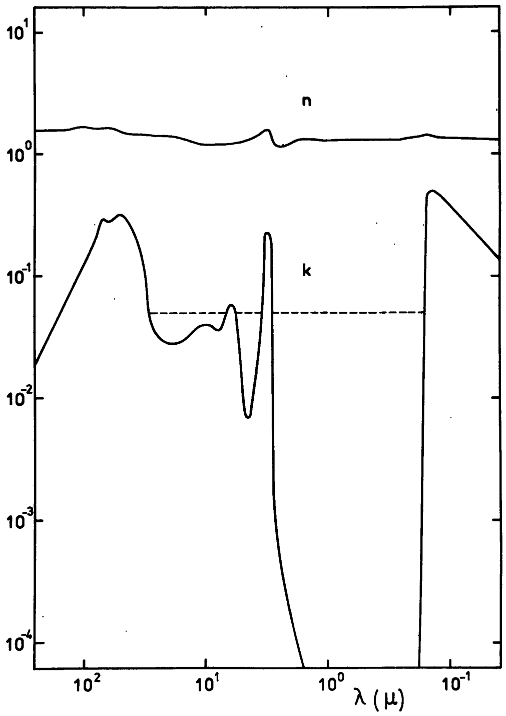


**Fig. 3.** The adopted optical constants of ice and dirty ice (dashed line)

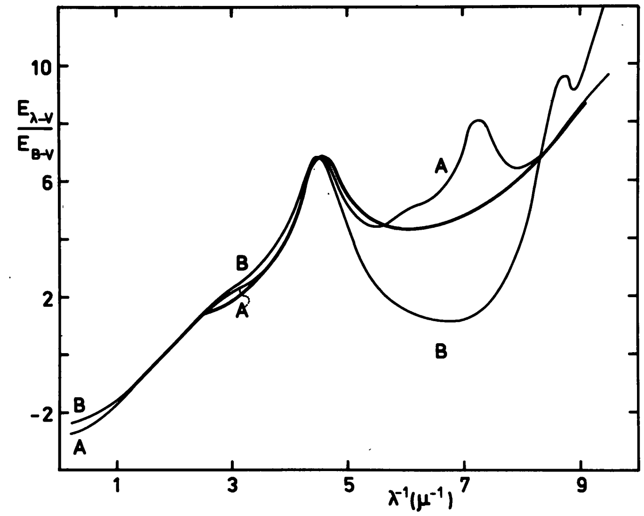


**Fig. 4.** Calculated extinction curves for models A and B (see Table 1). The heavy line is the average observed interstellar extinction curve (Bless and Savage, 1972)

---

approaches $n=1.57$ while the imaginary part is inversely proportional to $\lambda$, $k(\lambda)=6.5/\lambda(\mu)$. The observed 3.1 μ feature is very prominent in the $k$ curve. Ice is more transparent than silicate in particular in the visible, while absorptivities occur at longer wavelengths than in silicate. In our calculations we shall use a "dirty ice" material that is characterized by larger absorptivity ($k=0.05$) in the visible and near-infrared wavelength region (dashed line in Fig. 3).

For simplicity and in order not to increase the number of free parameters beyond control we further assume that each component of the dust consists of single size spherical particles. The number density and sizes of particles of each dust component is determined by fitting the observed extinction and albedo curves. In Fig. 4 we show the mean observed extinction curve, derived by Bless and Savage (1972) by averaging over a large number of stars. We also show our best fits for two dust models, A and B. The parameters of these two models are given in Table 1. The theoretical extinction curves are constructred with the relation

$$\frac{E(\lambda-V)}{E(B-V)}=\frac{\sum_{i=1}^{3} n_i\pi a_i^2[Q_{\mathrm{ext}}^{(i)}(a_i,\lambda)-Q_{\mathrm{ext}}^{(i)}(a_i,V)]}{\sum_{i=1}^{3} n_i\pi a_i^2[Q_{\mathrm{ext}}^{(i)}(a_i,B)-Q_{\mathrm{ext}}^{(i)}(a_i,V)]}$$

where $n_i$ and $a_i$ are the number density and the radius of dust particles of component $i$ ($1\equiv$graphite, $2\equiv$silicate, $3\equiv$ice) and $Q_{\mathrm{ext}}^{(i)}(a_i,\lambda)$ are the extinction efficiencies of particles of component $i$ calculated according to Mie theory (van de Hulst, 1957). The effective wavelengths of the $B$ and $V$ photometric filters are taken to be 4300 Å and 5500 Å, respectively (Allen, 1973). In fitting the average observed extinction curve we have five parameters $n_2/n_1$, $n_3/n_1$, $a_1$, $a_2$, and $a_3$ that can be varied. Several of these parameters can be determined more or less independently because

**Table 1.** Dust parameters

| Model | Parameters | Graphite | Silicate | Dirty ice |
|---|---|---|---|---|
| A | $a$ (Å) | 200 | 500 | 3000 |
| | Volume % | 7 | 18 | 75 |
| | $n/n_{\mathrm{H}}$ | $2.2\ 10^{-11}$ | $3.7\ 10^{-12}$ | $7.0\ 10^{-14}$ |
| B | $a$ (Å) | 200 | 50 | 2500 |
| | Volume % | 7 | 17 | 76 |
| | $n/n_{\mathrm{H}}$ | $2.1\ 10^{-11}$ | $3.1\ 10^{-9}$ | $1.1\ 10^{-13}$ |

different parts of the extinction curve are dominated by different dust components. The fits in Fig. 4 have been constructed subject to two constraints. First, we require that the curves pass exactly through the observed extinction maximum at $\lambda^{-1}=4.6\ \mu^{-1}$. This requirement determines the sizes and the relative amount of graphite particles (e.g. Gilra, 1972). Secondly we fix the relative amount of silicates by requiring that the observed ratio $W_{10}/A_V$ is reproduced, where $W_{10}$ is the equivalent width of the 9.7 μ interstellar absorption feature. From observations of the heavily reddened star VI Cygni nr. 12 by Rieke (1974) one derives $W_{10}/A_V=0.10$ μ. We assume that in spite of the difference in the shape of the 9.7 μ feature between terrestrial and interstellar silicates, the equivalent width of the feature is the same. At 9.7 μ we have $2\pi a_2/\lambda \ll 1$ for the silicate particle sizes in both models so that this constraint determines the relative amounts of silicate particles independent of the particle size.

In both models the infrared and visible extinction ($\lambda^{-1}\lesssim 3\ \mu^{-1}$) is dominated by ice particles, graphite explains the extinction in the inverse wavelength range $3\ \mu^{-1}\lesssim\lambda^{-1}\lesssim 5\ \mu^{-1}$. In model A the extinction in the range $5\ \mu^{-1}\lesssim\lambda^{-1}\lesssim 8\ \mu^{-1}$ is due to silicates, while for $\lambda^{-1}\gtrsim 8\ \mu^{-1}$ graphite once again dominates. This model has the disadvantage that the extinction levels off at $\lambda^{-1}\simeq 9\ \mu^{-1}$ in conflict with the observations of York et al. (1973). Model B follows a suggestion by Greenberg and Hong (1974) that the continued rise of the extinction in the far-ultraviolet can be

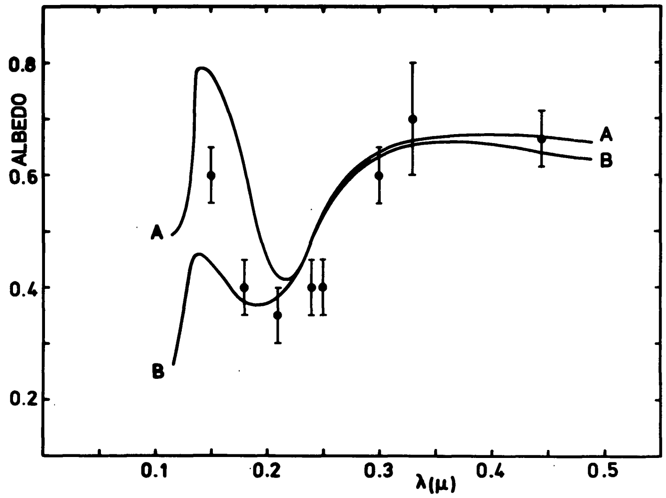


**Fig. 5.** Calculated albedo curves for models A and B (see Table 1). The observations shown are from Lillie and Witt (1976)

explained by very small silicate particles. Indeed the curves in Fig. 4 show that model B rises more steeply at very short wavelengths, but it fails to reproduce the observed extinction in the range $5\,\mu^{-1} \lesssim \lambda^{-1} \lesssim 8\,\mu^{-1}$. It is conceivable that a more realistic approach with some distribution of silicate particle sizes would produce a more satisfactory fit. A distribution of silicate particle sizes would also smear out the humps at $7.2\,\mu^{-1}$ in model A and at $8.8\,\mu^{-1}$ in model B. Both are due to the silicate absorption edge at about 1200 Å (see Fig. 2). The hump in curve A reflects the anomalous dispersion peak in $n$ ($Q_{\text{ext}} \simeq Q_{\text{sca}}$ for 500 Å particles) and the hump in curve B, which occurs at much shorter wavelengths, is due to the peak in $k$ ($Q_{\text{ext}} \simeq Q_{\text{abs}}$ for 50 Å particles). The value of $R = A_v/E_{B-V}$, which is exclusively determined by ice in both models, equals 2.8 in model A and 2.4 in model B [$E(\lambda - V)/E(B-V)$ at $\lambda^{-1} = 0$ in Fig. 4], while observations give $R \simeq 3$ (Johnson, 1968).

In Fig. 5 we show the observed values of the albedo of the dust according to the recent analysis of Lillie and Witt (1976) together with the calculated albedos for the two dust models in Table 1. The theoretical albedo curves are constructed from the relation

$$\varpi(\lambda) = \frac{\sum_{i=1}^{3} n_i \pi a_i^2 Q_{\text{sca}}^{(i)}(a_i, \lambda)}{\sum_{i=1}^{3} n_i \pi a_i^2 Q_{\text{ext}}^{(i)}(a_i, \lambda)}$$

where $Q_{\text{sca}}^{(i)}$ is the scattering efficiency of dust particles of component $i$ and the other quantities have the same meaning as before. The shape of the calculated albedo curves is in reasonable agreement with the observations of Lillie and Witt (1976). The strong minimum in the albedo curve at the wavelength of the extinction maximum is due to graphite absorption. The theoretical curves are somewhat too high in the wavelength range between 2000 Å and 3000 Å probably due to the fact that the relative amount of graphite is somewhat too small. The peaks in both albedo curves around 1400 Å are caused by the silicate absorption edge. We believe that a particle size distribution would result in smearing the peaks and in an albedo curve somewhere intermediate between A and B.

The absolute number densities of the particles in Table 1 have been derived from the relative number densities with the use of the

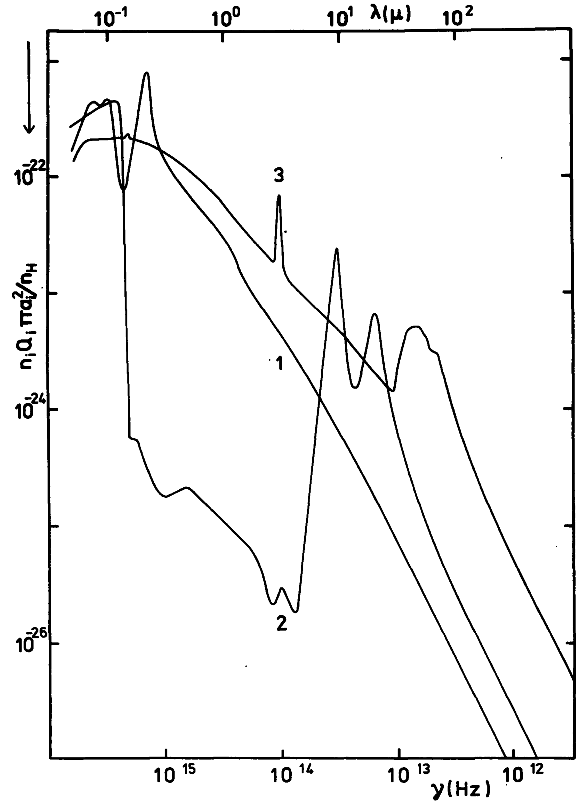


**Fig. 6.** Calculated absorption cross sections of graphite (1), silicate (2), and dirty ice (3) particles for model A per Hydrogen atom in the gas

relation $N_H/E_{B-V} = 5\;10^{21}\,\text{cm}^{-2}\,\text{mag}^{-1}$ (Bohlin, 1975). Adopting specific weights of graphite, silicate, and ice of 2.5, 2.5, and 1 g cm$^{-3}$, respectively, we find from the number densities in Table 1 a dust-gas ratio of 0.87% by mass for model A and 0.82% for model B. The total amount of C, O, and Si atoms in our dust models does not violate the cosmic abundances of these elements (Allen, 1973). In Fig. 6 we show the absorption coefficients of our dust model A per Hydrogen atom as a function of frequency. These absorption coefficients are calculated from the optical properties in Figs. 1–3 and the abundances and sizes in Table 1.

The main uncertainty in our dust model is the presence of ice in the interstellar dust. The strength of the 3.1 μ absorption band in the spectra of several objects suggest that at most 20% of the mass of interstellar dust is in the form of ice, a factor 3 less than in our model (Merrill et al., 1976). Thus ice is not the main component of the interstellar dust. On the other hand observations of the interstellar linear and circular polarization strongly suggest that only dielectric particles can self-consistently explain the observations at visible wavelengths (Martin, 1974). The most plausible solution of this problem is provided by a dust component with a composition similar to that originally put forward by van de Hulst (1949) which consists of some combination of the hydrides of Carbon, Nitrogen, and Oxygen with all kinds of impurities. Several arguments can be put forward to explain why only a small fraction of the total number of Oxygen atoms in the dust is available for the observed 3.1 μ OH stretching band (e.g. Greenberg, 1976). Whatever the exact composition of the dirty ice-like component, we emphasize that for our purpose the most important properties are (i) that it is dielectric in the visible and (ii) that its absorptivity in the ultraviolet and in the infrared are of similar strength and occur at similar wavelengths as in ice. The first property determines the visible extinction and polarization, the second property regulates the temperature that ice grains will attain inside an H II region. Another uncertainty in our dust model is the size of the silicate particles. As discussed before it is impossible to reproduce simultaneously the near- and the far-ultraviolet extinction and albedo curves with single-size silicate particles.

## 3. Ionization Structure of a Dusty H II Region

We have extended the numerical methods of Hummer and Seaton (1963, 1964) to solve the ionization structure of a spherical H II region containing Hydrogen and Helium gas to also include the effects of dust particles. We splitted the ionizing radiation field in two parts (i) the stellar photons, and (ii) the diffuse photons. For the stellar photons we may write down two differential radiative transfer equations

$$\frac{dS_{\rm H}^*}{dr}=-\varkappa_d S_{\rm H}^*-\varkappa_{\rm H}\xi_{\rm H}S_{\rm H}^* \tag{1}$$

and

$$\frac{dS_{\rm He}^*}{dr}=-\varkappa_d' S_{\rm He}^*-\varkappa_{\rm H}'\xi_{\rm H}S_{\rm He}^*-\varkappa_{\rm He}'\xi_{\rm He}S_{\rm He}^*. \tag{2}$$

Where $\xi_{\rm H}$ and $\xi_{\rm He}$ are the neutral fractions of Hydrogen and Helium respectively, $S_{\rm He}^*$ is the photon emission rate of stellar photons that can ionize Hydrogen and Helium ($\lambda<504$ Å) and $S_{\rm H}^*$ is the photon emission rate of stellar photons that can ionize Hydrogen only (504 Å $<\lambda<$ 912 Å). We assume that Helium is singly ionized. Since we are dealing with stars with temperatures below 50,000 K this is a good approximation. The quantities $\varkappa_{\rm H}$ and $\varkappa_{\rm H}'$ are the absorption coefficients of Hydrogen for H and He ionizing photons, respectively, averaged over the stellar radiation field

$$\varkappa_{\rm H}=n_{\rm H}\langle\sigma_{\rm H}\rangle=n_{\rm H}\int_{504}^{912}\frac{S^*(r,\lambda)}{S_{\rm H}(r)}\sigma_{\rm H}(\lambda)d\lambda,$$

$$\varkappa_{\rm H}'=n_{\rm H}\langle\sigma_{\rm H}'\rangle=n_{\rm H}\int_{228}^{504}\frac{S^*(r,\lambda)}{S_{\rm He}(r)}\sigma_{\rm H}(\lambda)d\lambda,$$

where

$$\sigma(\lambda)=6.3\ 10^{-18}\left(\frac{\lambda(\text{Å})}{912}\right)^3\ \text{cm}^2$$

(Hummer and Seaton, 1963).
The quantity $\varkappa_{\rm He}'$ is the averaged absorption coefficient of Helium for Helium ionizing photons

$$\varkappa_{\rm He}'=n_{\rm He}\langle\sigma_{\rm He}'\rangle=n_{\rm He}\int_{228}^{504}\frac{S^*(r,\lambda)}{S_{\rm He}^*(r)}\sigma_{\rm He}(\lambda)d\lambda$$

where

$$\sigma_{\rm He}(\lambda)=7.35\ 10^{-18}\exp\left(-0.73\left(\frac{912}{\lambda(\text{Å})}-1.807\right)\right)\ \text{cm}^2$$

(Hummer and Seaton, 1964).
The quantities $\varkappa_d$ and $\varkappa_d'$ are the averaged absorption coefficients of the dust for H and He ionizing photons respectively defined as follows

$$\varkappa_d=\sum_{i=1}^{3}n_i\pi a_i^2\int_{504}^{912}Q_{\rm abs}^{(i)}(\lambda)S^*(r,\lambda)d\lambda/S_{\rm H}^*(r)$$

and

$$\varkappa_d'=\sum_{i=1}^{3}n_i\pi a_i^2\int_{228}^{504}Q_{\rm abs}^{(i)}(\lambda)S^*(r,\lambda)d\lambda/S_{\rm He}^*(r)$$

where $n_i$, $a_i$, and $Q_{\rm abs}^{(i)}$ are dust parameters that have been discussed in the previous section (cf. Table 1). All the absorption coefficients are in principle a function of position in the nebula. However, as long as the Hydrogen optical depth for H ionizing photons is not much larger than unity the spectral energy distribution of the radiation field does not change, so that the values of $\varkappa_{\rm H}(r)$, $\varkappa_{\rm H}'(r)$, $\varkappa_{\rm He}'(r)$, $\varkappa_d(r)$, and $\varkappa_d'(r)$ will not differ markedly from their value at $r=0$. We shall assume that all absorption coefficients are constant over the H II region.

The formal solutions of Eqs. (1) and (2) are

$$S_{\rm H}^*(r)=S_{\rm H}^*(0)\exp(-\tau_{\rm H}) \tag{3}$$

and

$$S_{\rm He}^*(r)=S_{\rm He}^*(0)\exp(-\tau_{\rm He}) \tag{4}$$

where $\tau_{\rm H}$ and $\tau_{\rm He}$, the optical depth for Hydrogen and Helium ionizing photons respectively, are defined by the differential equations

$$\frac{d\tau_{\rm H}}{dr}=\varkappa_d+\varkappa_{\rm H}\xi_{\rm H} \tag{5}$$

and

$$\frac{d\tau_{\rm He}}{dr}=\varkappa_d'+\varkappa_{\rm H}'\xi_{\rm H}+\varkappa_{\rm He}'\xi_{\rm He} \tag{6}$$

with the boundary condition $\tau_{\rm H}=\tau_{\rm He}=0$ at the inner boundary.

There are also two differential radiative transfer equations for the diffuse photons resulting from recombinations of Hydrogen and Helium

$$\frac{dS_{\rm H}^D}{dr}=-\varkappa_{\rm H}\xi_{\rm H}S_{\rm H}^D-\varkappa_d S_{\rm H}^D+4\pi r^2(\alpha_{\rm H}^{(1)}-\alpha_{\rm H}^{(2)})n_e n_{\rm H}(1-\xi_{\rm H})$$
$$+4\pi r^2\alpha_{\rm He}^{(2)}n_e n_{\rm He}f(1-\xi_{\rm He}) \tag{7}$$

and

$$\frac{dS_{\rm He}^D}{dr}=-\varkappa_{\rm H}'\xi_{\rm H}S_{\rm He}^D-\varkappa_{\rm He}'\xi_{\rm He}S_{\rm He}^D-\varkappa_d'S_{\rm He}^D$$
$$+4\pi r^2(\alpha_{\rm He}^{(1)}-\alpha_{\rm He}^{(2)})n_e n_{\rm He}(1-\xi_{\rm He}). \tag{8}$$

$S_{\rm H}^D$ is the photon emission rate of diffuse photons that can ionize Hydrogen only. This diffuse radiation field consists of photons resulting from direct recombination to the ground level of Hydrogen and of photons originating from $n=2$ in Helium, of which only a fraction $f$ is energetic enough to ionize Hydrogen. In our numerical calculations we adopt $f=0.69$, the value at $n_{\rm H}=10^4$ cm$^{-3}$ (Osterbrock, 1974). $S_{\rm He}^D$ is the photon emission rate of diffuse photons from direct recombination to the ground level of Helium. These photons can ionize Hydrogen and Helium. $\alpha_{\rm H}^{(n)}$ and $\alpha_{\rm He}^{(n)}$ are the recombination coefficients to all level down to the $n^{th}$ level for Hydrogen and Helium respectively. We have assumed that the average absorption coefficients of Hydrogen, Helium and of the dust for the diffuse photons are the same as for the stellar photons.

In order to solve the ionization equilibrium we use the so-called "on the spot approximation"

$$\frac{dS_{\rm H}^D}{dr}=\frac{dS_{\rm He}^D}{dr}=0. \tag{9}$$

We first assume that the Hydrogen diffuse radiation field is only absorbed on the spot by Hydrogen and the Helium radiation field is only absorbed by Helium and that no diffuse photons are absorbed by the dust (Hummer and Seaton, 1963; OSA of Petrosian and Dana, 1975). Then combining Eqs. (7)–(9) with the equations of ionization equilibrium for Hydrogen

$$(1-\xi_{\mathrm{H}})4\pi r^2\alpha_{\mathrm{H}}^{(1)}n_e n_{\mathrm{H}}=\varkappa_{\mathrm{H}}\xi_{\mathrm{H}}(S_{\mathrm{H}}^D+S_{\mathrm{H}}^*)+\varkappa_H'\xi_{\mathrm{H}}(S_{\mathrm{He}}^D+S_{\mathrm{He}}^*) \tag{10}$$

and Helium

$$(1-\xi_{\mathrm{He}})4\pi r^2\alpha_{\mathrm{He}}^{(1)}n_e n_{\mathrm{He}}=\varkappa_{\mathrm{He}}'\xi_{\mathrm{He}}(S_{\mathrm{He}}^D+S_{\mathrm{He}}^*) \tag{11}$$

we find

$$\xi_{\mathrm{H}}=\varepsilon[C_{\mathrm{H}}-C_{\mathrm{He}}f(1-\xi_{\mathrm{He}})]/(\varkappa_{\mathrm{H}}S_{\mathrm{H}}^*+\varkappa_{\mathrm{H}}'S_{\mathrm{He}}^*+C_{\mathrm{H}}\varepsilon) \tag{12}$$

and

$$\xi_{\mathrm{He}}=\varepsilon C_{\mathrm{He}}/(\varkappa_{\mathrm{He}}'S_{\mathrm{He}}^*+C_{\mathrm{He}}\varepsilon) \tag{13}$$

where we have followed Hummer and Seaton in defining the quantities

$$C_{\mathrm{H}}(r)=4\pi r^2\alpha_{\mathrm{H}}^{(2)}n_{\mathrm{H}}^2 \quad \text{and} \quad C_{\mathrm{He}}(r)=4\pi r^2\alpha_{\mathrm{He}}^{(2)}y_{\mathrm{He}}n_{\mathrm{H}}^2$$

and the reduced electron density

$$\varepsilon(r)=n_e/n_{\mathrm{H}}=(1-\xi_{\mathrm{H}})+y_{\mathrm{He}}(1-\xi_{\mathrm{He}})$$

where $y_{\mathrm{He}}$ is the Helium abundance by number. Next we allow for the fact that H and He diffuse photons can be absorbed on the spot by the dust and by Hydrogen (GOSA of Petrosian and Dana, 1975). Using the definitions of $C$ and $\varepsilon$ above we find the following diffuse radiation fields from Eqs. (7)–(9)

$$S_{\mathrm{H}}^D=\frac{C_{\mathrm{H}}\varepsilon[(\alpha_{\mathrm{H}}^{(1)}/\alpha_{\mathrm{H}}^{(2)})-1]\,(1-\xi_{\mathrm{H}})+C_{\mathrm{He}}\varepsilon(1-\xi_{\mathrm{He}})f}{\varkappa_{\mathrm{H}}\xi_{\mathrm{H}}+\varkappa_d} \tag{14}$$

and

$$S_{\mathrm{He}}^D=\frac{C_{\mathrm{He}}\varepsilon\,[(\alpha_{\mathrm{He}}^{(1)}/\alpha_{\mathrm{He}}^{(2)})-1]\,(1-\xi_{\mathrm{He}})}{\varkappa_{\mathrm{H}}'\xi_{\mathrm{H}}+\varkappa_{\mathrm{He}}'\xi_{\mathrm{He}}+\varkappa_d'}. \tag{15}$$

Inserting the radiation fields again in the equations of ionization equilibrium (10) and (11) we obtain the final values of $\xi_{\mathrm{H}}$ and $\xi_{\mathrm{He}}$

$$\xi_{\mathrm{H}}=\frac{C_{\mathrm{H}}\varepsilon\alpha_{\mathrm{H}}^{(1)}/\alpha_{\mathrm{H}}^{(2)}}{\varkappa_{\mathrm{H}}(S_{\mathrm{H}}^*+S_{\mathrm{H}}^D)+\varkappa_{\mathrm{H}}'(S_{\mathrm{He}}^*+S_{\mathrm{He}}^D)+C_{\mathrm{H}}\varepsilon\alpha_{\mathrm{H}}^{(1)}/\alpha_{\mathrm{H}}^{(2)}} \tag{16}$$

and

$$\xi_{\mathrm{He}}=\frac{C_{\mathrm{He}}\varepsilon\alpha_{\mathrm{He}}^{(1)}/\alpha_{\mathrm{He}}^{(2)}}{\varkappa_{\mathrm{He}}'(S_{\mathrm{He}}^*+S_{\mathrm{He}}^D)+C_{\mathrm{He}}\varepsilon\alpha_{\mathrm{He}}^{(1)}/\alpha_{\mathrm{He}}^{(2)}}. \tag{17}$$

Effectively our solution boils down to one iteration step in an iterative solution of Eqs. (14)–(17) with starting values of $\xi_{\mathrm{H}}$ and $\xi_{\mathrm{He}}$ given by Eqs. (12) and (13).

The numerical integration of the two coupled differential Eqs. (5) and (6) together with their boundary conditions is carried out with the use of a fourth-order Runge-Kutta integration technique. For some combination of the parameters $\tau_{\mathrm{H}}$, $\tau_{\mathrm{He}}$ and the radial coordinate $r$, we first find $S_{\mathrm{H}}^*$ and $S_{\mathrm{He}}^*$ from Eqs. (3) and (4). Then assuming some starting value for $\varepsilon(r)$, we calculate $\xi_{\mathrm{H}}$ and $\xi_{\mathrm{He}}$ according to the procedure defined above, and finally the values of the derivatives follow from Eqs. (5) and (6). Each Runge-Kutta integration step is repeated until the reduced electron density $\varepsilon(r)$ has converged to within one percent.

We have checked the accuracy of our on the spot approximation by comparing our results with the more exact calculations of the ionization structure of H II regions by Mathis (1971). We have calculated the ratio of the volumes of the Helium and of the Hydrogen Strömgren spheres around exciting stars with black-body spectra assuming that there is no dust inside the H II region. Our results agree within 5% with Mathis' results. Another check of our numerical results consists of calculating the fraction of the ultraviolet photons absorbed by the gas as a function of the dust optical depth $\tau_d$ in H II regions. These results agree within 10% with the calculations by Mathis (1971).

## 4. Heating Function

The temperature of a dust particle $T_d$ at distance $r$ of the central star is determined by balancing the emission and absorption of radiation

$$4\pi a^2\int_0^\infty Q_{\mathrm{abs}}(\nu)\pi B(\nu,T_d)d\nu=\pi a^2\left[\int_0^\infty Q_{\mathrm{abs}}(\nu)\frac{L_*(\nu)}{4\pi r^2}\exp(-\tau(r,\nu))d\nu\right.$$
$$\left.+4\pi\int_0^\infty Q_{\mathrm{abs}}(\nu)J^D(r,\nu)d\nu+4\pi\int_0^\infty Q_{\mathrm{abs}}(\nu)J^N(r,\nu)d\nu\right]. \tag{18}$$

The first term on the right-hand side describes the heating of the dust particle by direct stellar photons, the second term describes the heating due to diffuse photons emitted by the gas which are absorbed on the spot (ionizing photons and resonantly scattered Lyman $\alpha$ photons), the third term describes the heating due to diffuse photons which are absorbed throughout the whole cloud (cooling photons and recombination photons other than Ly $\alpha$). These three terms together will be referred to as the heating function.

### 4.1. Stellar Photons

The photons of the direct stellar radiation field can be divided in Helium (and Hydrogen) ionizing photons (228 Å$<\lambda<$504 Å), Hydrogen ionizing photons (504 Å$<\lambda<$912 Å) and non-ionizing photons ($\lambda>$912 Å). The first term on the right-hand side of Eq. (18) can then be splitted up as follows

$$\int_0^\infty Q_{\mathrm{abs}}(\nu)\frac{L^*(\nu)}{4\pi r^2}\exp(-\tau(r,\nu))d\nu=Q_{\mathrm{H}}\frac{S_{\mathrm{H}}^*(r)}{4\pi r^2}\langle h\nu\rangle_{\mathrm{H}}^*$$
$$+Q_{\mathrm{He}}\frac{S_{\mathrm{He}}^*(r)}{4\pi r^2}\langle h\nu\rangle_{\mathrm{He}}^*+\int_0^{\nu_1}Q_{\mathrm{abs}}(\nu)\frac{L^*(\nu)}{4\pi r^2}\exp(-\tau(r,\nu))d\nu$$

where $Q_{\mathrm{H}}$, $\langle h\nu\rangle_{\mathrm{H}}^*$, $Q_{\mathrm{He}}$, and $\langle h\nu\rangle_{\mathrm{He}}^*$ are averages of $Q_{\mathrm{abs}}$ and of $h\nu$ over the Hydrogen and Helium ionizing part of the stellar radiation field, respectively. We shall assume that these averages are constant throughout the H II region. The frequency $\nu_1$ is the Lyman continuum frequency. The stellar photon emission rates $S_{\mathrm{H}}^*$ and $S_{\mathrm{He}}^*$ are taken from the numerical solution of the ionization structure described in Sect. 3. The non-ionizing stellar photons heat the dust throughout the whole cloud.

### 4.2. Diffuse Photons

With diffuse photons we mean resonantly scattered recombination photons, i.e. Helium (and Hydrogen) ionizing recombination photons, Hydrogen ionizing recombination photons and Hydrogen Lyman $\alpha$ photons (see Sect. 3). These photons are assumed to be absorbed on the spot. The second term in Eq. (18) can be split up accordingly

$$4\pi\int_0^\infty Q_{\mathrm{abs}}(\nu)J^D(r,\nu)d\nu=Q_{\mathrm{H}}\frac{S_{\mathrm{H}}^D(r)}{4\pi r^2}\langle h\nu\rangle_{\mathrm{H}}^D+Q_{\mathrm{He}}\frac{S_{\mathrm{He}}^D(r)}{4\pi r^2}\langle h\nu\rangle_{\mathrm{He}}^D$$
$$+f_\alpha Q_\alpha\alpha_{\mathrm{H}}^{(2)}n_e n_{\mathrm{H}}(1-\xi_{\mathrm{H}})h\nu_\alpha/\varkappa_\alpha.$$

The diffuse ionizing stellar photon rates $S_{\mathrm{H}}^{D}$ and $S_{\mathrm{He}}^{D}$ and the neutral fraction $\xi_{\mathrm{H}}$ are taken from the numerical solution of the ionization structure in Sect. 3. We have again assumed that the averages of $Q_{\mathrm{abs}}(\nu)$ over the diffuse radiation field and over the direct stellar radiation field are the same. The mean photon energies $\langle h\nu\rangle_{\mathrm{H}}^{D}$ and $\langle h\nu\rangle_{\mathrm{He}}^{D}$ are equal to the sum of the ionization potential of H and He and the mean kinetic energy of the electrons in the H II region. In this way we neglect the excess energy of the Helium Ly $\alpha$ photons which can ionize Hydrogen. This leads to underestimating the energy in the diffuse Hydrogen ionizing radiation field by about 2%. In the Hydrogen Lyman $\alpha$ heating term $Q_{\alpha}$ is the absorption efficiency of the dust particle at 1208 Å, $\varkappa_{\alpha}^{-1}$ is the mean free path of Lyman $\alpha$ photons for absorption by dust particles, $f_{\alpha}$ is the fraction of Hydrogen recombinations to levels $n \geqq 2$ ending up as Ly $\alpha$ photons and $h\nu_{\alpha}$ is the energy of the Lyman $\alpha$ photon. At a density of $n=10^4$ cm$^{-3}$ we find $f_{\alpha}=0.80$, the remaining 20% is emitted in the Hydrogen two-photon continuum (Osterbrock, 1974).

### 4.3. Nebular Photons

These photons are created by the ionized gas and not absorbed on the spot but throughout the whole cloud. We shall subsequently treat forbidden line radiation, Hydrogen two-photon emission and Hydrogen and Helium recombinations other than Ly $\alpha$. The last term in Eq. (18) can be written formally

$$4\pi \int_0^{\infty} Q_{\mathrm{abs}}(\nu) J^{N}(r,\nu)\,d\nu = 2\pi \int_{-1}^{1}\int_0^{\infty}\int_0^{\infty} Q_{\mathrm{abs}}(\nu) j_N(r',\nu) \cdot \exp\left(-\tau(l,\nu)\right) d\nu\, dl\, d\mu \tag{19}$$

where $j_N(r',\nu)$ is the volume emissity at $r'$ and the integration is along rays $l$ over all direction cosines $\mu$, while $r'$ is defined by $r'=(r^2+l^2-2lr\mu)^{1/2}$ and $\tau$ is the optical depth along $l$. In practice we use average $Q$ values for each kind of nebular photons. Equation (19) can thus be rewritten

$$4\pi \int_0^{\infty} Q_{\mathrm{abs}}(\nu) J_N(r,\nu)\,d\nu = 2\pi \int_{-1}^{1}\int_0^{\infty} \langle Q\rangle j_N(r') \exp\left(-\tau(l)\right) dl\, d\mu \tag{20}$$

where

$$\langle Q\rangle = \int_0^{\infty} Q_{\mathrm{abs}}(\nu) j_N(r,\nu)\,d\nu / j_N(r), \qquad j_N(r) = \int_0^{\infty} j_N(r,\nu)\,d\nu$$

and

$$\tau(l) = \int_0^{l} n_d(r')\pi a^2 \langle Q\rangle\, dl'.$$

We have assumed that $\langle Q\rangle$ does not change with position in the cloud. We now derive $j_N(r,\nu)$ for each kind of nebular radiation.

a) Forbidden Line Radiation

The dominant cooling line of H II regions is the doublet of [O II] $\lambda\lambda$ 3726–3729 Å (Osterbrock, 1974). We assume that all energy given to the ionized gas by photo-ionization of Hydrogen and Helium is radiated in this line. Thus

$$\begin{aligned}4\pi j_N(r) &= \varkappa_{\mathrm{H}}\xi_{\mathrm{H}} \frac{S_{\mathrm{H}}^{*}(r)}{4\pi r^2}\left(\langle h\nu\rangle_{\mathrm{H}}^{*} - I_{\mathrm{H}} - kT_e\right)\\ &+ \varkappa_{\mathrm{H}}'\xi_{\mathrm{H}} \frac{S_{\mathrm{He}}^{*}(r)}{4\pi r^2}\left(\langle h\nu\rangle_{\mathrm{He}}^{*} - I_{\mathrm{H}} - kT_e\right)\\ &+ \varkappa_{\mathrm{He}}'\xi_{\mathrm{He}} \frac{S_{\mathrm{He}}^{*}(r)}{4\pi r^2}\left(\langle h\nu\rangle_{\mathrm{He}}^{*} - I_{\mathrm{He}} - kT_e\right)\\ &+ \varkappa_{\mathrm{H}}'\xi_{\mathrm{H}} \frac{S_{\mathrm{He}}^{D}}{4\pi r^2}\left(I_{\mathrm{He}} - I_{\mathrm{H}}\right)\end{aligned}$$

where $I_{\mathrm{H}}$ and $I_{\mathrm{He}}$ are the ionization potentials of Hydrogen and Helium, respectively and $kT_e$ is the mean kinetic energy of the electrons. $\langle Q\rangle$ in Eq. (20) is defined as $\langle Q\rangle = Q$ (3700 Å). All other symbols have been defined in Sect. 3.

b) Hydrogen Two-photon Continuum

A fraction $(1-f_{\alpha})$ of the Hydrogen recombinations to levels with $n \geqq 2$ will decay through the Hydrogen two-photon continuum ($2^2S-1^1S$). These photons have a mean energy of $h\nu_{\alpha}/2=5.1$ eV. Thus we have

$$4\pi j_N(r) = 2(1-f_{\alpha}) n_e n_{\mathrm{H}} (1-\xi_{\mathrm{H}}) \alpha_{\mathrm{H}}^{(2)} h\nu_{\alpha}/2\,.$$

$\langle Q\rangle$ in Eq. (20) is now averaged over the spectral energy distribution of the two-photon continuum (Spitzer and Greenstein, 1951).

c) Hydrogen Recombination Photons

For every Hydrogen recombination to levels $n \geqq 2$ on the average an amount of energy $(I_{\mathrm{H}} - h\nu_{\alpha} + kT_e)$ ends up in the recombination photon field. Then

$$4\pi j_N(r) = n_e n_{\mathrm{H}} (1-\xi_{\mathrm{H}}) \alpha_{\mathrm{H}}^{(2)} (I_{\mathrm{H}} - h\nu_{\alpha} + kT_e)$$

and since the intensity weighted average wavelength of the recombination photons is about 5000 Å we take $\langle Q\rangle = Q$ (5000 Å).

d) He Recombination Photons

We recognize three different ways in which He recombination photons contribute to the heating function. Firstly, all He recombinations down to $n=2$ can be accounted for by one photon of mean energy $\langle h\nu\rangle_1 = 5.4$ eV per recombination. Every He recombination produces one such photon ($f_1=1$).

Secondly, He Lyman $\alpha$ photons ($n=2\rightarrow 1$) consist of two contributions A fraction $f_2$ of all Helium recombinations down to $n=2$ produces one two-photon continuum photon with mean energy $\langle h\nu\rangle_2 = 4.4$ eV. (The complementary photon that can ionize Hydrogen has already been accounted for in the diffuse Hydrogen ionizing radiation field.)

A fraction $f_3$ of all He recombinations down to $n=2$ produces two two-photon continuum photons with total energy $\langle h\nu\rangle_3 = 20.7$ eV neither of which can ionize Hydrogen.

The volume emissivity due to He recombination photons can be written separately for each contribution to the heating function

$$4\pi j_N = \alpha_{\mathrm{He}}^{(2)} n_e n_{\mathrm{He}} (1-\xi_{\mathrm{He}}) f_j \langle h\nu\rangle_j \qquad j=1, 2, 3.$$

In our numerical calculations we adopt $f_2=0.48$ and $f_3=0.31$, the values of these parameters at $n_{\mathrm{H}}=10^4$ cm$^{-3}$ (Osterbrock, 1974). For the three kinds of He recombination photons we have $\langle Q\rangle_1 = Q$ (2300 Å), $\langle Q\rangle_2 = Q$ (2800 Å), and $\langle Q\rangle_3 = Q$ (1200 Å), which have to be inserted in Eq. (20).

It is to be understood that all relations derived in this section apply to graphite, silicate, and ice particles separately.

**Table 2.** Model parameters

| Model | $T_{\rm eff}$(K) | $\delta$ | $A_V$(mag) | $\tau_d$ | $f_{\rm gas}$ | $L_*/L_\odot$ | $L_{1-40}/L_\odot$ | $L_{40-350}/L_\odot$ |
|---|---|---|---|---|---|---|---|---|
| I | 50,000 | 1 | 23 | 1.6 | 0.34 | 1.3 $10^6$ | 6.9 $10^5$ | 1.4 $10^5$ |
| II | 50,000 | 0.1 | 23 | 0.14 | 0.90 | 4.9 $10^5$ | 2.0 $10^5$ | 1.0 $10^5$ |
| III | 50,000 | 0.01 | 23 | 0.014 | 0.99 | 4.5 $10^5$ | 1.6 $10^5$ | 1.0 $10^5$ |
| IV | 35,000 | 0.01 | 23 | 0.014 | 0.99 | 1.1 $10^6$ | 6.3 $10^5$ | 2.1 $10^5$ |

## 5. Description of the Model

We consider a spherical H II region of uniform density with radius $R_{II}$ ionized by a central O star. Inside the H II region is a central cavity with radius $R_0$ devoid of gas and dust. For the energy distribution of the star we use the non-LTE models of Mihalas (1976) with $\log g = 4.0$. Due to its higher pressure an H II region expands into the surrounding medium and therefore develops a high density shell of swept-up material. We assume that the density in this circumstellar shell is hundred times larger than the density of the ionized gas (e.g. Mathews, 1969). Furthermore we assume that all of the extinction is produced by this shell. The thickness of the shell is then related to the amount of visual extinction $A_v$. Typically for $A_v \simeq 25$ the thickness of the shell is about 0.1 times the radius of the H II region.

There are three kinds of dust grains in the cloud, graphite, silicate, and ice, and we adopt the sizes and relative abundances derived from the interstellar extinction and albedo curves in Sect. 2 (see Table 1). The density of dust in the cloud still remains to be specified. There is accumulating evidence that the dust inside H II regions is underabundant with respect to the general interstellar medium although the amount of depletion is still controversial (e.g. Panagia, 1974; de Jong et al., 1975; Natta and Panagia, 1976). The dust may be depleted in several ways, (i) it may be driven out of the center of the H II region by radiation pressure (hole in the center with radius $R_0$), (ii) the amount of dust may be reduced throughout the H II region with a factor $\delta$, for instance by sputtering (iii) the dust may evaporate when its temperature rises above the sublimation temperature $T_{\rm ev}$ (probably only of importance for ice where $T_{\rm ev} \simeq 100$ K).

The parameters in our model are the Hydrogen number density $n_{\rm H}$, the Helium abundance $y_{\rm He}$, the electron temperature $T_e$, the radius of the H II region $R_{II}$, the inner radius of the shell $R_0$, the effective temperature $T_{\rm eff}$, and the luminosity $L_*$ of the central star, the visual extinction $A_v$ in the circumnebular shell, the depletion parameter $\delta$ and the evaporation temperature of ice $T_{\rm ev}$. Once these parameters are specified the ionization structure of the H II region and the heating function of the dust are calculated as described in Sects. 3 and 4. Then the dust temperatures are calculated from Eq. 18 and the infrared volume emissivity of the dust follows from

$$j_d(r,\nu) = \sum_{i=1}^{3} \varkappa_i(r,\nu) B(\nu, T_d^{(i)}) = \sum_{i=1}^{3} n_i(r) \pi a_i^2 Q_{\rm abs}^{(i)}(\nu) B(\nu, T_d^{(i)}) \quad (21)$$

where the summation is over the three kinds of dust particles discussed above. The infrared volume emissivity of the gas due to free-free and free-bound transitions of Hydrogen equals (e.g. Aller and Liller, 1968)

$$j_{ff}(r,\nu) = 5.4\ 10^{-39}\ T_e^{-1/2} \exp\left(-\frac{h\nu}{kT}\right) \cdot \bar{g}_{III} n_e n_{\rm H}(1-\xi_{\rm H})\ \text{erg cm}^{-3}\ \text{s}^{-1}\ \text{Hz}^{-1}\ \text{sterad}^{-1} \quad (22)$$

and

$$j_{bf}(r,\nu) = 1.72\ 10^{-33}\ T_e^{-3/2} \sum_n n^{-3} \exp\left[(h\nu_n - h\nu)/kT\right] \cdot \bar{g}_{II} n_e n_{\rm H}(1-\xi_{\rm H})\ \text{erg cm}^{-3}\ \text{s}^{-1}\ \text{Hz}^{-1}\ \text{sterad}^{-1} \quad (23)$$

where $h\nu_n$ is the energy of the $n^{th}$ Hydrogen level. In Eq. (23) the summation extends over all levels with energies smaller than $h\nu$. We take $\bar{g}_{II} = 1$, while $\bar{g}_{III}$ is found by interpolation in the tables published by Karzass and Latter (1961). The total infrared volume emissivity equals

$$j(r,\nu) = j_d(r,\nu) + (1 + y_{\rm He}) j_{ff}(r,\nu) + j_{bf}(r,\nu) \quad (24)$$

where the factor $(1 + y_{\rm He})$ takes account of the contribution of free-free emission by singly-ionized helium. The infrared intensity at a projected distance $r$ from the center of the cloud is

$$I(r,\nu) = \int_l j(r',\nu) \exp(-\tau(l',\nu))\, dl' \quad (25)$$

where the integration is along the line of sight $l$ with impact parameter $r$. The optical depth $\tau$ is measured along the line of sight towards the observer from some point in the cloud to the edge of the cloud. It has been shown by Mathis (1972) that $\tau$ should be the absorption optical depth. Finally the infrared flux density through an area with radius $r$ received at distance $D \gg r$ equals

$$F(r,\nu) = \frac{2\pi}{D^2} \int_0^r r' I(r',\nu)\, dr'. \quad (26)$$

## 6. A Model for W 3 A/IRS 1

We shall attempt to construct a model that fits the observations of the well-studied compact H II region W3 A/IRS1. This source is part of a very young complex consisting of compact H II regions, infrared sources and OH/$H_2O$ maser sources embedded in a dense molecular cloud. It has been mapped in great detail at radio wavelengths by Wynn-Williams (1971) and Harris and Wynn-Williams (1976), at near-infrared wavelengths by Wynn-Williams et al. (1972), Dyck and Simon (1976), Willner (1977), and Hackwell et al. (1978) and at far-infrared and millimeter wavelengths by Emerson et al. (1973), Harper (1974), Fazio et al. (1975), Furniss et al. (1975), and Westbrook et al. (1976). Both the near-infrared and the radio surface brightness distributions of W3 A/IRS1 show a strikingly similar incomplete shell structure with a radius of about 2/3 of the radius of the ionized region (Wynn-Williams et al., 1972). This clearly establishes the co-existence of gas and dust inside the H II region. Furthermore it has been shown that the gas is ionized by two O stars (IRS2 and IRS2a) of which IRS2 produces 90% of the ionizing photons (Harris and Wynn-Williams, 1976). Due to the poor spatial resolution at far-infrared wavelengths the individual sources, detected at near-infrared and radio wavelengths, are unresolved in the far-infrared

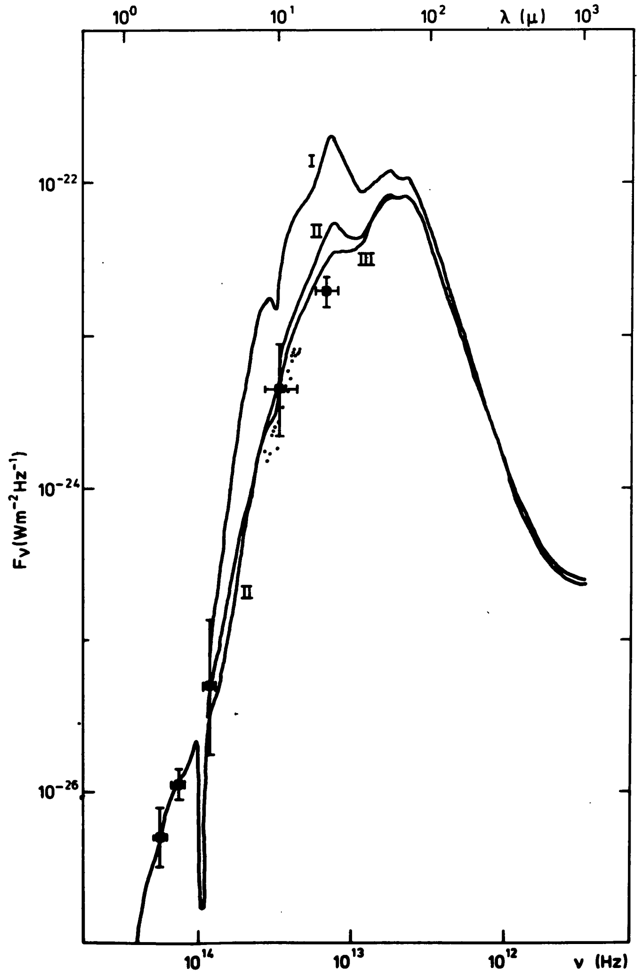


**Fig. 7.** The calculated infrared spectrum for models I, II and III. Observations shown are from Wynn-Williams et al. (1972, squares) and Willner (1977, dots)

maps. Throughout our discussion we shall use a distance of 3.0 kpc for W3A/IRS1. We assume that $T_e=10^4$ K and that $y_{\rm He}=0.1$. From the radio observations we know that $R_{II}=0.29$ pc, that $R_0=2/3\ R_{II}$ and that $n_{\rm H}=6700$ cm$^{-3}$. From these numbers we derive the total number of photons needed to ionize the gas. By choosing a value for the depletion parameter $\delta$, the optical depth of the dust for ionizing photons, $\tau_d$, can be calculated. The total number of ionizing photons emitted by the central star can then be estimated. If we choose an effective temperature, the luminosity of the star is found from the requirement that it produces the right number of ionizing photons. Since $\tau_d$ depends on the temperature of the dirty ice particles, because these particles evaporate at temperatures above $T_{\rm ev}$, a trial and error procedure has to be followed to theoretically obtain the right radio flux and size of the H II region. For our calculations we have adopted $T_{\rm ev}=100$ K.

We have calculated the infrared spectrum integrated over the whole source of four different models. For each model, the values adopted for $T_{\rm eff}$, $\delta$ and $A_v$ and the values derived for $\tau_d$, $L_*$, the 1–40 μ luminosity $L_{1-40}$, and the 40–350 μ luminosity $L_{40-350}$ are given in Table 2. In Fig. 7 we compare the infrared spectrum of three models, (I, II and III) with the near-infrared observations of W3A/IRS1. The observations at 1.65, 2.2, 3.6, 10, and 20 μ are taken from Wynn-Williams et al. (1972). The bandwidths and the error bars are as indicated. The 8–13 μ spectrophotometry has been taken from Willner (1977) who normalized his observations to the 10 μ flux of Wynn-Williams et al. The errors in his observations are typically about 10%. Dyck and Simon (1977) observed W3A/IRS1 at 8.4, 11.2, 12.8, 20, 25, and 33 μ with a 30″ aperture and a 30″ throw. Because of the small aperture size and the small throw their fluxes are lower limits to the total flux of W3A/IRS1. Their observed spectrum peaks around 20 μ. The shape of the spectrum around 10 μ is consistent with the spectroscopic results of Willner (1977). However, the ratio of the 20 μ to 10 μ flux is about a factor 2 larger than in the observations of Wynn-Williams et al. (1972). Dyck and Simon attribute this difference to a slightly larger effective wavelength at 20 μ or to better atmospheric conditions during their observations. Because of these uncertainties and because they observe the radiation of only part of the whole source we shall give low weight to the observations of Dyck and Simon in the comparisons with our models. Their observations are not shown in Fig. 7.

Models I, II, and III differ in the amount of dust present in the H II region. In model I, in which the dust is undepleted, the optical depth of the dust inside the H II region for ionizing photons is of the order of unity. Therefore, this dust absorbs a large fraction of the ionizing photons so that a central star with a high luminosity is required (see Table 2). This causes the dust in the ionized region to be too hot, so that too much energy is emitted in the near-infrared. In model II the dust is depleted by a factor 0.1 and $\tau_d$ is now much less than unity. Consequently the stellar luminosity is much lower than in model I. Because Lyman alpha photons are resonantly scattered the number of Lyman alpha photons absorbed by one dust particle increases when the number of dust particles decreases. The heating of the dust particles inside the H II region by Lyman alpha photons is now about equal to the heating by stellar photons. In model III the dust is depleted by a factor 0.01. The dust particles inside the H II region are now mainly heated by resonantly scattered Lyman alpha photons. Because of its near-infrared spectrum model I is completely ruled out by the observations. The near-infrared spectra of model II and III are in much better agreement with the observations although the 20 μ flux is still somewhat too high. Depleting the dust inside the H II region with an even larger factor will not lower it, because the flux at 20 μ is mainly emitted by dust in the neutral shell surrounding the H II region. Because of the idealized nature of our model and because of the observational uncertainties we will not give too much weight to this discrepancy and merely conclude that the dust optical depth for ionizing photons should be low ($\tau_d \lesssim 0.1$) and that therefore the dust inside the H II region has to be depleted by a factor of at least 0.1.

We note that the spectrum calculated for an aperture diameter of 30″ peaks around 20 μ similar to the observations of Dyck and Simon (1977) but that the calculated spectrum is systematically higher than observed by them. As mentioned before this difference could well be due to systematic errors in the observations.

In Fig. 8 we compare the infrared spectra of models III and IV with the observations. These models have the same depletion parameters, but the central star in model IV has a much lower effective temperature. Because the radio data are used as constraints for our models, the star with the lower effective temperature has a higher luminosity to produce the same number of ionizing photons (see Table 2). The dust temperature in model IV is therefore generally higher. The result is an overall higher flux and a small shift towards shorter wavelengths. The 20 μ flux in model IV is a factor 5 too high compared with the observed 20 μ flux. Thus the effective temperature of the central star cannot be as low

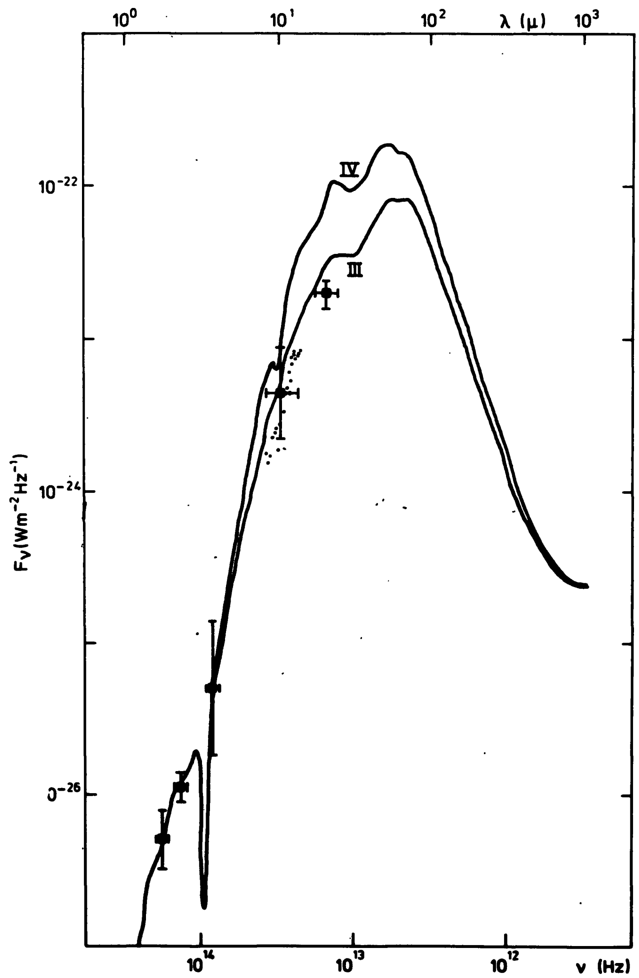


**Fig. 8.** The calculated spectrum for models III and IV. Observations from same authors as in Fig. 7

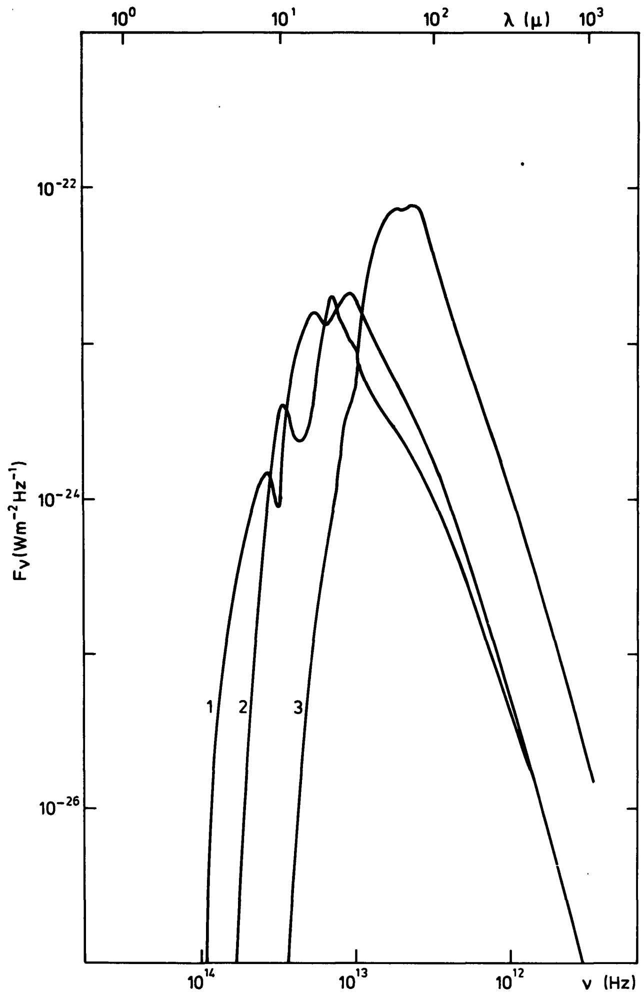


**Fig. 9.** The decomposed spectrum of model III. (1 = graphite, 2 = silicate, 3 = dirty ice)

as 35,000 K. Moreover, a high effective temperature is in agreement with the observation of the S IV emission line at 10.5 μ in W3A/IRS1 (Willner, 1977).

The observed infrared spectrum of an H II region is much broader than a black-body spectrum. It has been known that this is partly due to the temperature gradient of the dust particles through the cloud (Wright, 1973) and partly due to the coexistence of particles of different materials and consequently with different temperatures at each point in the cloud (Natta and Panagia, 1976). In Fig. 9 we have separated the infrared spectrum of model III, in which the dust inside the H II region is depleted by a factor 0.01, into the contributions from the different materials present in the cloud. Since graphite particles emit less efficiently in the far-infrared than silicate or ice particles (see Fig. 7), the temperature of the graphite particles is generally higher than the temperatures of the silicate and ice particles. The graphite particles will thus dominate the near-infrared spectrum, roughly from 5–15 μ. Note that the structure in the graphite emission is produced by the 10 and 20 μ absorption features of silicate. Due to the presence of resonances the emission from the silicate and ice particles peaks at 10 and 20 μ, respectively at 45–60 μ. The effects of dust temperature gradients in the cloud can most clearly be demonstrated on the basis of the silicate emission, but is present in the emission of all materials. The silicate particles inside the H II region are mainly heated by resonantly scattered Lyman alpha radiation. Because of the resulting high temperature, ~220 K, most of their energy will be radiated through the 10 μ oscillator. The silicate grains in the neutral shell surrounding the H II region are only heated by the non-ionizing stellar photons and the cooling photons of the H II region. Their temperature is therefore much lower. They produce most of the 20 μ feature and the far-infrared shoulder.

In Fig. 10 we present the calculated brightness distributions of models I, II, and III at near-infrared and radio wavelengths. These curves are constructed from Eq. (25). For a comparison with the observations they should be convolved with the beam. Due to the assumed density distribution a shell structure is apparent at all near-infrared and radio wavelengths. The comparison of our calculations with the observations is complicated by the presence of small-scale density structure (~5″) in the ionized shell of W3A/IRS1 (e.g. Harris and Wynn-Williams, 1976). A detailed calculation including the effects of these clumps is outside the scope of our model but it is reassuring that the 6 cm observations of Wynn-Williams (1971) with a 7″ beam do give an average center to shell intensity ratio of about 2, equal to our calculated value. At 2 μ the emission is due to free-free and free-bound

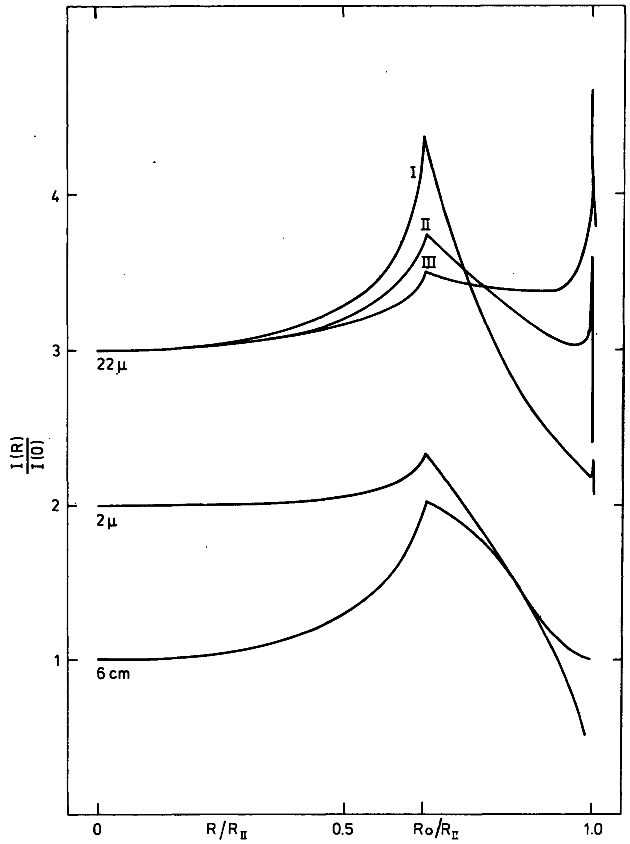


**Fig. 10.** The surface brightness normalized to the central surface brightness as a function of radius. The curves at different wavelengths are displaced by one unit

transitions in the ionized gas. The center to shell variation at 2 μ is less than at 6 cm. This is due to the variation in absorption in the neutral shell across the source and thus in fact due to the chosen geometry. The variation in absorption across the source also explains why the intensity distribution beyond $R=R_0$ drops off more rapidly at 2 μ than at 6 cm. At 22 μ the emission is due to dust grains. The center to shell variation in the brightness distribution at 22 μ is also smaller than at 6 cm due to the same effect. This is partly counterbalanced by the presence of a temperature gradient. In model III the dust in the ionized shell is mainly heated by resonantly scattered Lyman alpha radiation and has therefore an almost uniform temperature. In model II the heating by stellar photons is about equal to the Lyman alpha heating and in model I it is dominant. Therefore in these two models a temperature gradient is present (~15–30%) and the center to shell intensity variation is larger than in model III. The 20 μ observations of Hackwell et al. (1978) with a 12″ beam give a peak to center intensity ratio of 1.6. This would favor a model somewhere in between model II and III. But because of the uncertainty introduced by beam smearing effects and because the brightness distribution is also sensitive to the adopted geometry, we will merely conclude that our models II and III are also in reasonable agreement with the observed brightness distribution. In all depleted models the brightness distribution shows limb-brightening at wavelengths where the cloud is optically thin (roughly $\lambda \gtrsim 5$ μ). This is due to the high-density shell surrounding the H II region. At 20 μ the size of this shell is about 0″.05, and it scales approximately with the inverse of the density of this neutral shell. Because of the low spatial resolution (generally 5–10″) the limb-brightening will not show up in the observations but should be observable with increased spatial resolution. It should be noted that such a high-density shell always makes the 20 μ size equal to the radio size.

We next turn to a discussion of the far-infrared spectrum. The H II region W 3 (main component) has been observed in several broad wavelength bands in the far-infrared (Emerson et al., 1973; Harper, 1974; Fazio et al., 1975, and Furniss et al., 1975). Our models give a much lower far-infrared flux than observed. There are two reasons for this. First of all in our simple-minded treatment of the radiative transfer we assume that infrared radiation can be neglected as a heat source for the dust. This assumption breaks down at large optical depths in the cloud where infrared radiation is the only heat source remaining. Therefore, our assumption affects the temperature of the cool dust particles in the outer parts of the cloud, which give rise to the far-infrared emission. As can be seen in Table 2, in all of our models about 40% of the total energy is not properly accounted for due to this assumption. Secondly, because of the beam size (typically ~1′–4′) the far-infrared measurements will include contributions from all objects observed in the near-infrared by Wynn-Williams et al. (1972) in W 3 (main-component). The far-infrared luminosity should therefore be of the order of the luminosity of a cluster of early-type stars rather than of one single early-type star. It is therefore not surprising that the luminosity of the central star in our best fits, ~5 $10^5$ $L_\odot$, is lower than the observed total infrared luminosity, ~1.5–2 $10^6$ $L_\odot$. To check, whether our models of W3A/IRS1 are consistent with the observations of W 3 (main component), we calculated the total luminosity of a cluster of early-type stars, normalized to one O 5 star. Using the stellar birth rate function of Ostriker et al. (1974) and the luminosities of early-type stars as tabulated by Panagia (1973), we find that the luminosity of such a cluster is 2 $10^6$ $L_\odot$. The Lyman continuum photon flux of such a cluster would be 9.2 $10^{49}$ $s^{-1}$. It should be kept in mind that we are dealing with small numbers of stars and that statistical deviations could thus be of importance. The total luminosity of W 3 (main component) is consistent with such a cluster, but the observed total number of ionizing photons, is only 4.2 $10^{49}$ $s^{-1}$. We attribute this lack of ionizing photons to the source W 3/IRS 5. On the basis of the observed near-infrared spectrum and an attenuation factor derived from the 10 μ absorption feature, the intrinsic luminosity of this object has been estimated to be at least 5 $10^5$ $L_\odot$ (Aitken and Jones, 1973; Willner, 1977). Nevertheless, the object has not been detected at 5 GHz [S(5 GHz) < $10^{-28}$ $Wm^{-2}$ $Hz^{-1}$ according to Harris and Wynn-Williams, 1976]. If we assume that W 3/IRS 5 is an O 5 main sequence star, as suggested by its luminosity, then the size of the ionized region should be less than 0.002 pc and its density higher than $10^7$ $cm^{-3}$ in order to remain undetected at 6 cm. In fact the presence of an $H_2O$ maser is indicative of even higher densities (de Jong, 1973). Furthermore, if this source is a dust-embedded protostellar object we do not expect that the radius of the ionized region is much larger than the melting radius of the grains, typically $10^{14}$–$10^{15}$ cm (Bedijn et al., 1978). Thus it is likely that the ratio of the infrared luminosity to the Lyman continuum photon flux of W 3 (main component) is overestimated by about a factor 2 due to the presence of this source. It is clear that higher resolution (10″–20″) far-infrared observations could be extremely useful in the interpretation of the nature of the sources in W 3 (main component).

It is of some interest to discuss the circum-nebular extinction in the shell around W3A. In the depleted models the flux shortward of 3 μ is due to free-free and free-bound transitions in the ionized gas. This flux is strongly absorbed by the surrounding dust-shell. By fitting the observed flux at these wavelengths we derive an absorption optical depth at 2.2 μ, averaged over the source, equal to 1.7. According to our model calculations this averaged absorption optical depth corresponds to a radial visual extinction in the neutral shell of $A_v = 23$ mag. Using a dust model due to van de Hulst (1949, his curve nr. 15) and assuming that the attenuation at 2.2 μ is due to extinction (absorption and scattering) Wynn-Williams et al. (1972) derive $A_v \simeq 16$ mag. It has been shown by Mathis (1972) that the attenuation of the emergent flux from an H II region is determined by absorption rather than by extinction as assumed by Wynn-Williams et al. (1972). However, the main difference between their result ($A_v = 16$ mag) and ours ($A_v = 23$ mag) is due to the use of quite different dust models. We note that using van de Hulst (1949) curve nr. 15, as is common practice among observers, apparently leads to underestimating the extinction.

The amount of circumstellar extinction in W3A can also be determined from the attenuation of the central star W3A/IRS2 and 2a. Harris and Wynn-Williams (1976) obtained $A_v = 14$, once again on the basis of van de Hulst (1949) curve nr. 15. According to Mathis (1972) there is an important difference with the nebular case. In the nebular case the optical depth is an average over the source, while in the stellar case it is measured along the line of sight towards the star. Thus stellar photons may be scattered back into the beam by dust particles in the shell so that the optical depth towards the star will be somewhere in between the absorption and the extinction optical depths. The precise value will depend on the geometry of the cloud and on the albedo and phase function of the dust. In order to properly treat this difference we should have solved the radiative transfer problem exactly and have included scattering. The spectrum of the central star adopted in our model is consistent with the observations of W3A/IRS2 (Wynn-Williams et al., 1972; Beetz et al., 1976) if the optical depth lies somewhere in between the absorption and the extinction optical depths.

It is of interest to compare our model fits of W3A/IRS1 with the fit by Krügel and Mezger (1975). They were unable to get a satisfactory fit of the near-infrared spectrum of W3A/IRS1, which is not surprising in view of their highly idealized dust model (one dust component with $Q_{abs} \alpha \lambda^{-1}$ in the infrared). Furthermore in their analysis Krügel and Mezger did put most weight on the far-infrared luminosity, which they estimated to be about half of the total infrared luminosity of W3 (main component). In our opinion they did not properly account for the far-infrared emission of W3/IRS5 and therefore inferred a too high luminosity for the exciting star of W3A/IRS1 ($\sim 9\ 10^5\ L_\odot$). Consequently, in order to arrive at the right radio size and spectrum, they then needed a high optical depth of the dust for ionizing photons and in fact an overabundance of dust inside the ionized shell.

We will now proceed to a discussion of the main uncertainties of our model for W3A/IRS1, namely the assumed density structure and the adopted dust model. The radio and near-infrared observations show that W3A/IRS1 consists of an ionized shell with a somewhat clumpy structure. The sizes of these clumps are of the order of a few arc s. Defining the filling factor $\Phi$ as the inverse of the fractional volume occupied by the clumped ionized gas, we estimate $\Phi \sim 5$ from the 6 cm contour map of Harris and Wynn-Williams (1976). We could be underestimating $\Phi$ severely if these clumps themselves consist of much smaller clumps. But such a hierarchical model seems a rather arbitrary assumption. A detailed calculation of such a clumpy model lies clearly outside the scope of our paper, but we can roughly estimate the effect of clumps in the following way. In a model for W3A/IRS1 in which the ionized shell consists of a number of high-density clumps, the average smeared out Hydrogen density will be lower ($n_H \propto \Phi^{-1/2}$). Therefore the mean dust optical depth for ionizing photons will be lower and a less luminous star is required to ionize the H II region. Consequently the near-infrared flux of such a model will be lower. We estimate that for a filling factor of 5 and no dust depletion the luminosity and consequently the 20 μ flux will be about a factor 2 lower than in model I. In order to bring the 20 μ flux of model I down by a factor 10 a filling factor of 100 is required (compare models I and II in Fig. 7 and Table 2). Such a filling factor seems very high. The presence of clumps in model III will not change the infrared spectrum much since the dust optical depth for ionizing photons is already quite low. It should be noted that by comparing the brightness ratio of the clumps and their immediate surroundings at near-infrared and radio wavelengths we can in principle infer whether the dust is mainly heated by resonantly scattered Lyman alpha photons or by stellar photons. Since the emission of the ionized gas is proportional to $n_e^2$ an equal ratio at 6 cm and 20 μ would point strongly towards heating of the dust by resonantly scattered Lyman alpha photons. For such an analysis 20 μ observations with a resolution of about 2″ are needed, which is possible with present-day techniques.

In Sect. 2 we discussed two dust models, which fit the interstellar extinction and albedo curve equally well/poorly. Model A with large silicate grains, $a \simeq 0.05$ μ and model B with small silicate grains, $a \simeq 0.005$ μ. The major difference between the two dust models is the far-ultraviolet opacity, which is about 3 times higher in model B than in model A. In the preceding paragraphs we have shown that in order to match the observed spectrum and surface brightness distribution, the optical depth of the dust for ionizing photons should be low, $\tau_d \lesssim 0.1$ in model A. This corresponds to $\delta \lesssim 0.1$. The same limit would imply $\delta \lesssim 0.03$ for model B. It should be noted that when the dust inside the ionized region is mainly heated by Lyman alpha photons ($\delta \sim 0.01$) the difference in the far-ultraviolet absorption coefficient is unimportant and model A and B give the same result.

In all our models a deep 3.1 μ absorption feature due to $H_2O$ ice is present. Such a feature is not or only weakly observed in the near-infrared spectra of compact H II regions, but it shows up quite strongly in the spectra of cocoon stars embedded in molecular clouds (Merrill et al., 1976). The 3.1 μ ice feature is too strong in our models because we assumed that the dirty-ice particles consist exclusively of $H_2O$ ice. In reality the dirty-ice material will be some mixture of predominantly H, C, N, and O, containing all kinds of radical and molecules. For our purpose it is important that the optical constants of materials consisting of these radicals and molecules are rather similar. In fact the models presented in our paper would be hardly affected if we had taken dirty-ice like material with $n \simeq 1.3$ at all wavelengths and $k \simeq 0.05$ for $\lambda \lesssim 50$ μ, a solid state absorption band with $k_{max} \simeq 0.5$ at $\lambda \simeq 50$ μ and $k \propto \lambda^{-1}$ for $\lambda \gtrsim 50$ μ (cf. de Jong et al., 1975).

In all models presented in this section we have assumed that dirty-ice particles evaporate when their temperature is above 100 K. Accidentally the radius of the region where dirty-ice particles evaporate approximately coincides with the radius of the ionized region in the depleted models. When we assume instead that the evaporation temperature of ice is much higher than 100 K, then the ice particles inside the H II region will become too hot ($\sim 200$ K) to radiate their energy in the far-infrared. In that case a slight redistribution of the near-infrared flux over frequency takes place, but the near-infrared spectrum does not change noticeably. When the evaporation temperature of dirty-ice is lower than

100 K the ice particles in all models are evaporated far out into the neutral shell. As a consequence the graphite and silicate particles will pick up more energy. The 10–30 μ flux will increase and the 40–100 μ flux will decrease (compare Fig. 9). We find that for $T_{ev}=50$ K the 20 μ flux increases with a factor 1.5. The observations do not exclude this possibility but it seems unlikely that the evaporation temperature of ice is as low as 50 K.

### 7. Conclusions

From a detailed comparison of our model calculations with infrared and radio observations of the well studied compact H II region W3A/IRS1 we draw the conclusions listed below. We believe that most of these conclusions apply more generally to compact H II regions as a class.

(i) The near-infrared emission at wavelengths shortward of 5 μ is due to free-free and free-bound transitions in the ionized gas, the emission in the wavelength range from 5 to 30 μ is predominantly due to graphite particles, silicate particles only contribute substantially at 10 μ and 20 μ where silicate material possesses strong solid state resonances, dirty ice particles dominate the infrared spectrum from 30 μ to about 1 mm where free-free emission of the ionized gas takes over again.

(ii) The spectrum is broader than a black-body spectrum because of the coexistence of particles of different materials attaining different temperatures and due to gradients in the dust temperature distribution.

(iii) The dust optical depth for ionizing photons in W3A/IRS1 is less than 0.1. This implies a depletion of the dust inside the H II region with at least a factor 0.1.

(iv) The observed far-infrared emission of W3 (main component) is only partly due to W3A/IRS1. A substantial fraction of the total observed far-infrared luminosity is probably contributed by W3A/IRS5. This renders the usual arguments for an almost normal dust to gas ratio in W3A, based on a comparison of the far-infrared and the radio luminosity, very uncertain. This conclusion is not much affected by the main shortcomings of our models, the uncertain optical properties of dirty ice, that dominates the far-infrared spectrum and the poor treatment of the radiative transfer, that violates flux conservation at far-infrared wavelengths.

*Acknowledgements.* The research described in this paper was started about 6 years ago while one of the authors (T. de J.) held a position at Harvard College Observatory. He gratefully acknowledges many stimulating discussions with Drs J. A. Frogel, S. E. Persson, and E. L. Wright. Both of us would like to thank Drs. P. J. Bedijn, and S. S. Hong for useful discussions on dust properties and on some numerical aspects of the problem. Finally we thank Dr H. J. Habing and Dr N. Panagia for their constructive critical remarks on earlier versions of this paper.

### References

Aitken, D.K., Jones, B.: 1973, *Astrophys. J.* **184**, 127
Allen, C.W.: 1973, Astrophysical Quantities, Athlone press, London
Aller, L.H., Liller, W.: 1968, *Stars and Stellar Systems* VII, eds. G. P. Kuiper and B. M. Middlehurst, Univ. of Chicago Press, Chicago, p. 483
Bedijn, P., Habing, H.J., de Jong, T.: 1978, *Astron. Astrophys.* **69**, 73
Becklin, E.E., Frogel, J.A., Neugebauer, G., Persson, S.E., Wynn-Williams, C.G.: 1973, *Astrophys. J.* **187**, L125
Becklin, E.E., Frogel, J.A., Kleinmann, D.E., Neugebauer, G., Persson, S.E., Wynn-Williams, C.G.: 1974, *Astrophys. J.* **187**, 487
Beetz, M., Elsässer, H., Poulakos, C., Weinberger, R.: 1976, *Astron. Astrophys.* **50**, 41
Bless, R.C., Savage, B.D.: 1972, *Astrophys. J.* **171**, 293
Bohlin, R.C.: 1975, *Astrophys. J.* **200**, 402
Dyck, H.M., Simon, T.: 1977, *Astrophys. J.* **211**, 421
Emerson, J.P., Jennings, R.E., Moorwood, A.F.M.: 1973, *Astrophys. J.* **184**, 401
Fazio, G.G., Kleinmann, D.E., Noyes, R.W., Wright, E.L., Zeilik, M., Low, F.J.: 1975, *Astrophys. J.* **199**, L177
Frogel, J.A., Persson, S.E.: 1974, *Astrophys. J.* **192**, 351
Furniss, I., Jennings, R.E., Moorwood, A.F.M.: 1975, *Astrophys. J.* **202**, 400
Garbuny, M.: 1965, Optical Physics, Academic Press, New York
Gillett, F.C., Forrest, W.J.: 1973, *Astrophys. J.* **179**, 483
Gilra, D.P.: 1971, *Nature* **229**, 237
Gilra, D.P.: 1972, Scientific results from OAO-2, ed. A. D. Code, Nasa SP-310, p. 295
Greenberg, J.M.: 1968, in *Stars and Stellar Systems,* VII, eds. G. P. Kuiper and B. M. Middlehurst, Univ. of Chicago Press, Chicago, p. 221
Greenberg, J.M.: 1976, *Astrophys. Space Sci.* **39**, 9
Greenberg, J.M., Hong, S.S.: 1974, in H II *regions and the galactic center*, ed. A. F. M. Moorwood, 8th ESLAB Symp., ESRO sp-105, p. 153
Hackwell, J.A., Gehrz, R.D., Smith, J.R., Briotta, D.A.: 1978, *Astrophys. J.* **221**, 797
Harper, D.A.: 1974, *Astrophys. J.* **192**, 557
Harper, D.A., Low, F.J.: 1971, *Astrophys. J.* **165**, L9
Harris, S., Wynn-Williams, C.G.: 1976, *Monthly Notices Roy. Astron. Soc.* **174**, 649
Hummer, D.G., Seaton, M.J.: 1963, *Monthly Notices Roy. Astron. Soc.* **125**, 437
Hummer, D.G., Seaton, M.J.: 1964, *Monthly Notices Roy. Astron. Soc.* **127**, 217
van de Hulst, H.C.: 1949, *Rech. Astron. Obs. Utrecht* **11**, part 2
van de Hulst, H.C.: 1957, Light scattering by small particles, J. Wiley and Sons Inc., New York
Jennings, R.E.: 1975, *Lecture Notes in Physics* **42**, 137
Johnson, H.L.: 1968, in *Stars and Stellar Systems,* VII, eds. G. P. Kuiper and B. M. Middlehurst, Univ. of Chicago Press, Chicago, p. 167
de Jong, T.: 1973, *Astron. Astrophys.* **26**, 297
de Jong, T.: 1976, *Mem. Soc. Astron. Ital.* **45**, 189
de Jong, T., Israel, F.P., Tielens, A.G.G.M.: 1975, *Lecture Notes in Physics* **42**, 123
Jura, M.: 1975, *Astrophys. J.* **197**, 375
Karzass, W.J., Latter, R.: 1961, *Astrophys. J. Suppl.* **6**, 167
Lillie, C.F., Witt, A.N.: 1976, *Astrophys. J.* **208**, 64
Martin, P.G.: 1974, *Astrophys. J.* **187**, 461
Mathews, W.G.: 1969, *Astrophys. J.* **157**, 583
Mathis, J.S.: 1971, *Astrophys. J.* **167**, 261
Mathis, J.S.: 1972, *Astrophys. J.* **176**, 651
Merrill, K.M., Russell, R.W., Soifer, B.T.: 1976, *Astrophys. J.* **207**, 763
Mihalas, D.: 1976, NCAR technical note, NCAR-TN/STR-76
Moorwood, A.F.M., Feuerbacher, B.: 1975, *Astrophys. Space Sci.* **34**, 137

Nandy, K., Thompson, G.I., Jamar, C., Monfils, A., Wilson, R.: 1975, *Astron. Astrophys.* **44**, 195
Natta, A., Panagia, N.: 1976, *Astron. Astrophys.* **50**, 191
Osterbrock, D.E.: 1974, Astrophysics of gaseous nebulae, Freeman and Company, San Francisco
Ostriker, J.P., Richstone, D.O., Thuan, T.X.: 1974, *Astrophys. J.* **188**, L87
Panagia, N.: 1973, *Astron. J.* **78**, 929
Panagia, N.: 1974, *Astrophys. J.* **192**, 221
Petrosian, V., Dana, R.A.: 1975, *Astrophys. J.* **196**, 733
Phillipp, H.R.: 1971, *J. Phys. Chem. Solids* **32**, 1935
Pollack, J.B., Toon, O.B., Khare, B.N.: 1973, *Icarus* **19**, 372
Pottasch, S.R.: 1974, *Astron. Astrophys.* **30**, 371
Rieke, G.H.: 1974, *Astrophys. J.* **193**, L81
Spitzer, L., Greenstein, J.L.: 1951, *Astrophys. J.* **114**, 407
Taft, E.A., Phillipp, H.R.: 1965, *Phys. Rev.* **138**, A197
Westbrook, W.E., Werner, M.W., Elias, J.H., Gezari, D.Y., Hauser, M.G., Lo, K.Y., Neugebauer, G.: 1976, *Astrophys. J.* **209**, 94
Willner, S.P.: 1977, *Astrophys. J.* **214**, 706
Woolf, N.J.: 1975, in the *Dusty Universe*, eds. G. B. Field and A. G. W. Cameron, Smithsonian Astrophysical Observatory, p. 59
Wright, E.L.: 1973, *Astrophys. J.* **185**, 569
Wynn-Williams, C.G.: 1971, *Monthly Notices Roy. Astron. Soc.* **151**, 397
Wynn-Williams, C.G., Becklin, E.E., Neugebauer, G.: 1972, *Monthly Notices Roy. Astron. Soc.* **160**, 1
York, D.G., Drake, J.F., Jenkins, E.B., Morton, D.C., Rogerson, J.B., Spitzer, L.: 1973, *Astrophys. J.* **182**, L1